AGU PUBLICATIONS

Geophysical Research Letters

RESEARCH LETTER
10.1002/2016GL071518

Key Points:
- The longitudinal structure of tropical rain in an aquaplanet model with a simple subtropical continent depends on model physics
- Zonal variance of ITCZ location decreases with increasing continent extent due to subtropical cloud response over ocean
- Relative strength of cloud SW and total LW important for whether Hadley circulation rainfall amplifies in one hemisphere

Supporting Information:
- Supporting Information S1

Correspondence to:
E. A. Maroon,
elizabeth.maroon@colorado.edu

Citation:
Maroon, E., and D. M. W.Frierson (2016), The impact of a continent's longitudinal extent on tropical precipitation, *Geophys. Res. Lett.*, *43*, 11,921–11,929, doi:10.1002/2016GL071518.

Received 9 JAN 2016
Accepted 10 NOV 2016
Accepted article online 15 NOV 2016
Published online 26 NOV 2016

The impact of a continent's longitudinal extent on tropical precipitation

Elizabeth A. Maroon[1] and Dargan M. W. Frierson[2]

[1]Cooperative Institute for Research in Environmental Sciences, University of Colorado Boulder, Boulder, Colorado, USA, [2]Department of Atmospheric Sciences, University of Washington, Seattle, Washington, USA

Abstract We examine how the longitudinal extent of a subtropical continent impacts the distribution of tropical precipitation in two aquaplanet general circulation models. In the simpler model, the addition of land decreases evaporation and precipitation in the hemisphere with the continent, and the precipitation response scales with the continent's extent. In the more comprehensive model, tropical precipitation has zonal variation due to the downstream response of clouds to land. As the continental extent increases, this cloud response weakens and the Intertropical Convergence Zone becomes more zonal and shifts to the continent. The different precipitation responses in the two models indicate the importance of radiative feedbacks in modifying tropical circulation in models.

1. Introduction

Tropical precipitation occurs where there is large-scale ascent, including the monsoon regions and in the Intertropical Convergence Zone (ITCZ). As such, the dynamics of monsoon and Hadley circulations are key to understanding the location of tropical precipitation. However, it is hard to disentangle these two circulations: for example, during the solsticial seasons, the bulk of the Hadley circulation occurs as part of the Asian monsoon circulation [*Dima and Wallace*, 2003]. Monsoon precipitation can thus be thought of as a seasonal displacement of the ITCZ over land, and theories that apply to the ITCZ can be applied to the monsoon [*Chao and Chen*, 2001; *Gadgil*, 2003; *Privé and Plumb*, 2007a; *Bordoni and Schneider*, 2008; *Merlis et al.*, 2013a].

There are two strong constraints on the zonal-mean tropical circulation: an angular momentum constraint [*Held and Hou*, 1980; *Lindzen and Hou*, 1988; *Plumb and Hou*, 1992; *Bordoni and Schneider*, 2008] and an energetic constraint [*Broccoli et al.*, 2006; *Kang et al.*, 2008, 2009; *Donohoe et al.*, 2013; *Frierson et al.*, 2013; *Schneider et al.*, 2014]. Angular momentum is nearly conserved when the Rossby number is large during the solstice seasons, but does not provide a constraint on the circulation strength [*Bordoni and Schneider*, 2008; *Merlis et al.*, 2013b]. The energetic constraint, when applicable [see *Kang et al.*, 2009; *Merlis et al.*, 2013b; *Shaw et al.*, 2015], does provide a constraint on circulation strength and the ITCZ location. Energy is transported from one hemisphere to the other by the upper branch of the Hadley circulation; by mass conservation, the lower branch transports moisture in the opposite direction. Because temperatures are constrained in the tropical free troposphere [*Sobel et al.*, 2001], temperature anomalies at the subtropical edge (which are connected to midlatitude energy transport by eddies) can affect energy transport and circulation through the entire Hadley regime. This relation between interhemispheric temperature gradients and tropical precipitation can be used to help diagnose shifts in zonal-mean tropical precipitation in the recent and deeper past [*Chiang and Bitz*, 2005; *Broccoli et al.*, 2006; *Frierson and Hwang*, 2012; *Hwang et al.*, 2013]. However, the confined zonal extent of monsoons limits the applicability of zonal-mean frameworks [*Privé and Plumb*, 2007b].

Simple model configurations are helpful for testing the applicability of zonal-mean frameworks to climate forcings that vary zonally. Understanding of tropical precipitation can be built by starting with aquaplanet simulations that have simple land geometries and then gradually increasing the geometry's complexity. In this study, we examine how the longitudinal extent of a subtropical continent alters the zonal and azonal precipitation response in two atmospheric general circulation models (GCMs). We focus on the energetic constraint discussed above and examine how continental extent affects the strength of monsoonal-Hadley circulations. Although orography is key for strengthening the Asian monsoon [see, e.g., *Hahn and Manabe*, 1975; *Boos and Kuang*, 2010], the continent's extent may also be important. In the following sections, we describe our model

configurations (section 2), examine the zonal-mean and zonally varying response of precipitation (section 3), and compare the results to previous studies (section 4).

2. Models

We add simple continents to two aquaplanet GCMs of differing complexity. The first model is the Gray Radiation Moist (GRaM) GCM, which includes the effect of latent heating by moisture, but does not include clouds or the radiative effect of water vapor [*Frierson et al.*, 2006]. The second model is the finite volume numerics Geophysical Fluid Dynamics Laboratory (GFDL) Atmospheric Model 2.1 (AM2.1), which has comprehensive physical parameterizations [*Geophysical Fluid Dynamics Laboratory Global Atmospheric Model Development Team*, 2004]; our simplified AM2.1 version was first configured by *Shi and Durran* [1992]. Annual mean insolation is used in both models; similar simulations with a seasonal cycle and varying land albedo are described in *Maroon et al.* [2016].

An aquaplanet simulation is used as the control for both models, and additional simulations have idealized subtropical continents that vary in longitudinal extent. In the AM2.1 control, the width of the ITCZ is narrow, and as a result, any precipitation shifts in AM2.1 simulations will be larger than that in GRaM (Figure S1 in the supporting information). All continents span from 10°N to 30°N, are flat, and at sea level. Two continental simulations were conducted with GRaM: a 60° continent simulation and a 360° continent simulation. AM2.1 simulations with continents have longitudinal extents of 60°, 120°, 180°, 240°, 300°, and 360°.

The albedo of all continents is set to the ocean's albedo in the subtropics; thus, there is no interhemispheric difference in net radiation due to surface albedo. Because GRaM does not have clouds, the ocean albedo is set to 0.29 to produce a more realistic energy budget. In AM2.1, the ocean albedo is approximately 0.06 in the subtropics. Both models use Land Model version 2 (LM2) [*Milly and Shmakin*, 2002], which is a bucket model based upon *Manabe* [1969]. The parameters used in LM2 for the two GCMs differ. See *Scheff* [2014] and *Maroon et al.* [2016] for further description of the models and these parameters.

Both models are coupled to a slab ocean with a mixed layer depth of 2.4 m and are spun up for 5 years, with an additional 5 years used for climatology. Control simulation precipitation (P), evaporation (E), and sea surface temperature (SST) are shown in Figure S1.

3. Results

3.1. GRaM Simulation Results

In both the 60° and 360° continent GRaM simulations, precipitation decreases over the continent, in the NH deep tropics south of the continent, and immediately north of the continent (Figure 1a, blue lines). The 60° simulation zonal-mean precipitation and evaporation changes (light blue and red lines in Figure 1a) are multiplied by 6 to compare with the 360° simulation. In the time- and zonal-mean moisture budget, these precipitation changes are balanced by changes in evaporation and moisture flux convergence. In the NH tropics and subtropics, the tropical precipitation change is mostly balanced by evaporation, and there is little import of SH moisture (Figure 1a, red lines). Evaporation decreases and sensible heating increases due to an unsaturated surface replacing the ocean. Surface temperature increases over land (Figure S2) due to a decrease in lower tropospheric moisture promoting a dry adiabatic lapse rate, while upper level temperatures are unchanged [*Joshi et al.*, 2008]. The heating from the continent drives lower tropospheric convergence (Figures 1b, 1c, and S2) at the continent's southern edge. Moisture is transported toward the continent and away from the ITCZ, decreasing precipitation on the northern side of the equator. Over the continent, the precipitation decrease is not as large as the evaporation decrease because of moisture convergence from this anomalous shallow circulation.

These precipitation and evaporation changes are zonally confined to the region with the continent. As a result, the response of zonal-mean precipitation and overturning circulation is largely proportional to continent's longitudinal extent (Figures 1a–1c). The majority of circulation changes are below 600 hPa, and there is not a significant stationary Rossby wave response in the tropics, although there is anomalous high sea level pressure to the northwest of the continent (Figure S3).

The hemispheric asymmetry (NH-SH) of precipitation and evaporation can be seen in Figure 1 and is quantified in Figures 2a and 2b. NH-SH precipitation and evaporation are calculated as the hemispheric difference of

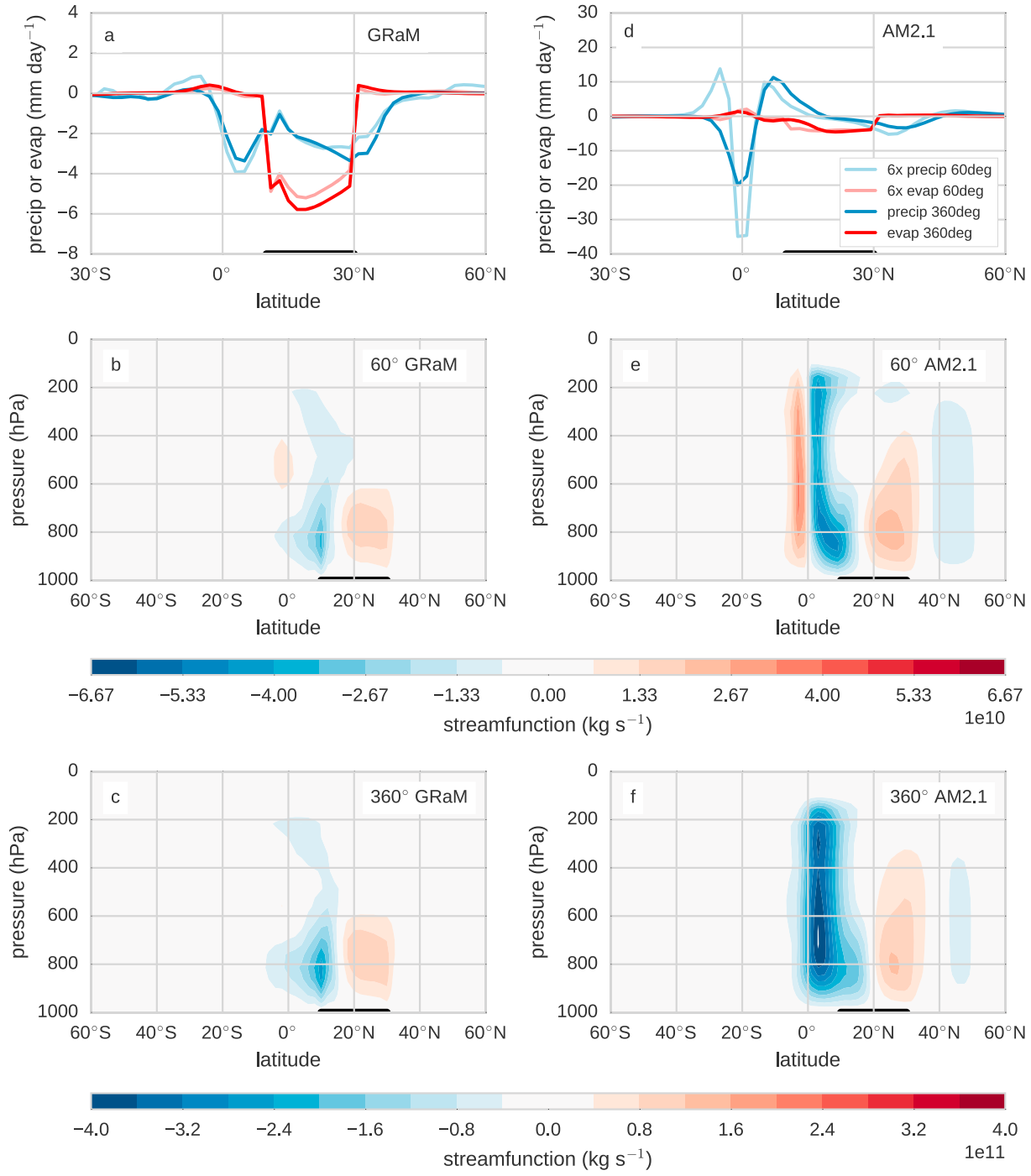

Figure 1. Changes in zonal-mean precipitation, evaporation, and overturning streamfunction in GRaM and AM2 simulations. (a) The changes in precipitation (blue) and evaporation (red) from simulations with 60° (light colors) and 360° (dark colors) continents. The anomalies for the 60° continent simulation are multiplied by six for comparison to the 360° simulations. (b, c) The change in overturning streamfunction for the 60° and 360° continent GRaM simulations. (d–f) Equivalent quantities for the AM2.1 simulations. Changes are relative to each model's aquaplanet simulation. The colormap for Figures 1c and 1f is 6 times greater than the colormap in Figures 1b and 1e. Black lines indicate the location of the continent.

the NH and SH area-averaged *P* or *E*. For both continents in GRaM, the change in NH-SH evaporation almost completely balances the change in zonal mean NH-SH precipitation (red circles, Figure 2a). Northward energy transport has increased and zonal mean *P-E* has shifted northward in the 360° simulation as compared to the 60° simulations (Figure 2b). If anomalous Hadley circulation mass transport were responsible for both the change in *P-E* and energy transport, these two quantities would be inversely related. Instead, the land-induced

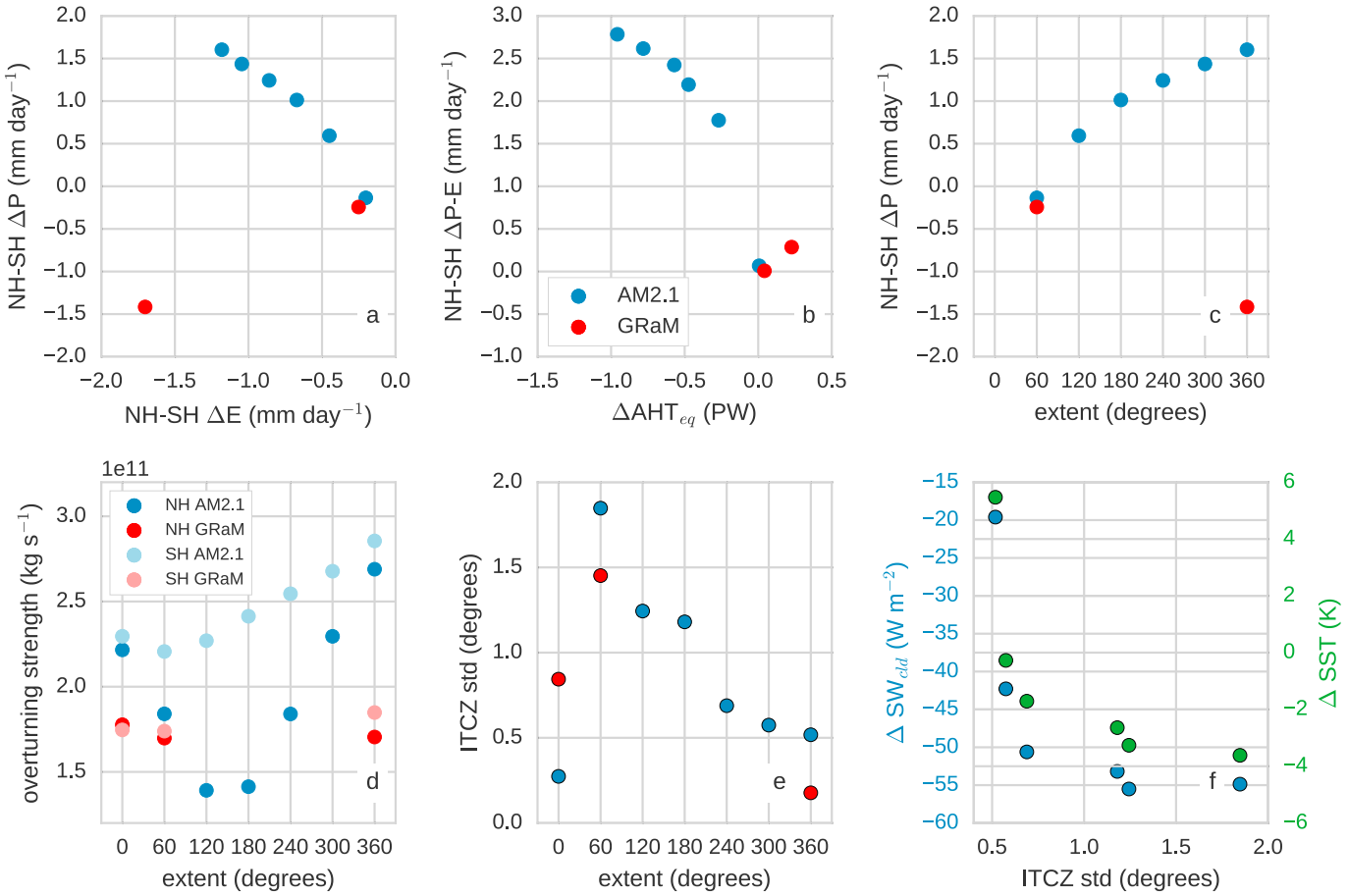

Figure 2. (a) Change in NH-SH zonal mean *P* versus *E* for GRaM (red) and AM2.1 (blue) simulations; (b) zonal mean change in *P-E* versus change in cross-equatorial atmospheric heat transport; and (c) change in zonal mean NH-SH *P* versus continental extent. (d) NH (dark colors) and SH (light colors) strength of the Hadley cells' overturning stream functions versus the longitudinal extent of the continent. (e) Standard deviation of ITCZ location versus continental extent. (f) Change in SW cloud radiative effect and SST in the region from 10°N–16°N and 90°E–105°E versus the standard deviation of the ITCZ location. Changes are relative to the aquaplanet simulations.

circulation change is shallow (Figures 1b and 1c), which alters the gross moist stability in this simulation. With a moist static energy minimum in the midtroposphere, there is negative gross moist stability in this bottom heavy circulation [*Back and Bretherton*, 2006]. This reverses the relation between equatorial energy transport and *P-E* that will be seen later in the AM2.1 simulations that have deep circulation changes.

The strength of the Hadley circulation in both hemispheres decreases in the 60° continent simulation, with the NH cell weaker than the SH cell. This difference in strength is larger in the 360° simulation (Figure 2d). The addition of the continent pulls the ascending region of the SH cell northward, and the region of peak ascent is north of the equator. When the Hadley circulation has off-equatorial ITCZ ascent, the cell in the hemisphere with the ITCZ is weaker than the cell in the other hemisphere [*Lindzen and Hou*, 1988].

3.2. AM2.1 Simulation Results

There are also hemispheric precipitation and evaporation changes in the deep tropics and NH subtropics of the AM2.1 simulations (Figures 1d–1f and Figure 2a, blue circles), but the climate responses are no longer zonally confined to the continental region as in the GRaM simulations (Figures 3 and S4). Precipitation shifts are larger than those in the GRaM simulations because of the sharper ITCZ in the AM2.1 simulations (Figure S1). Regardless of the continent's extent, land evaporation decreases by almost the same amount as in the GRaM simulations, again because of decreased surface water availability. The higher land surface temperature in AM2.1 induces surface convergence at the continent's southern edge, again like the GRaM simulations (Figures 1e and 1f). In AM2.1, however, the anomalous land-driven circulation is deeper in the vertical than in GRaM, and it crosses the equator (Figure S2).

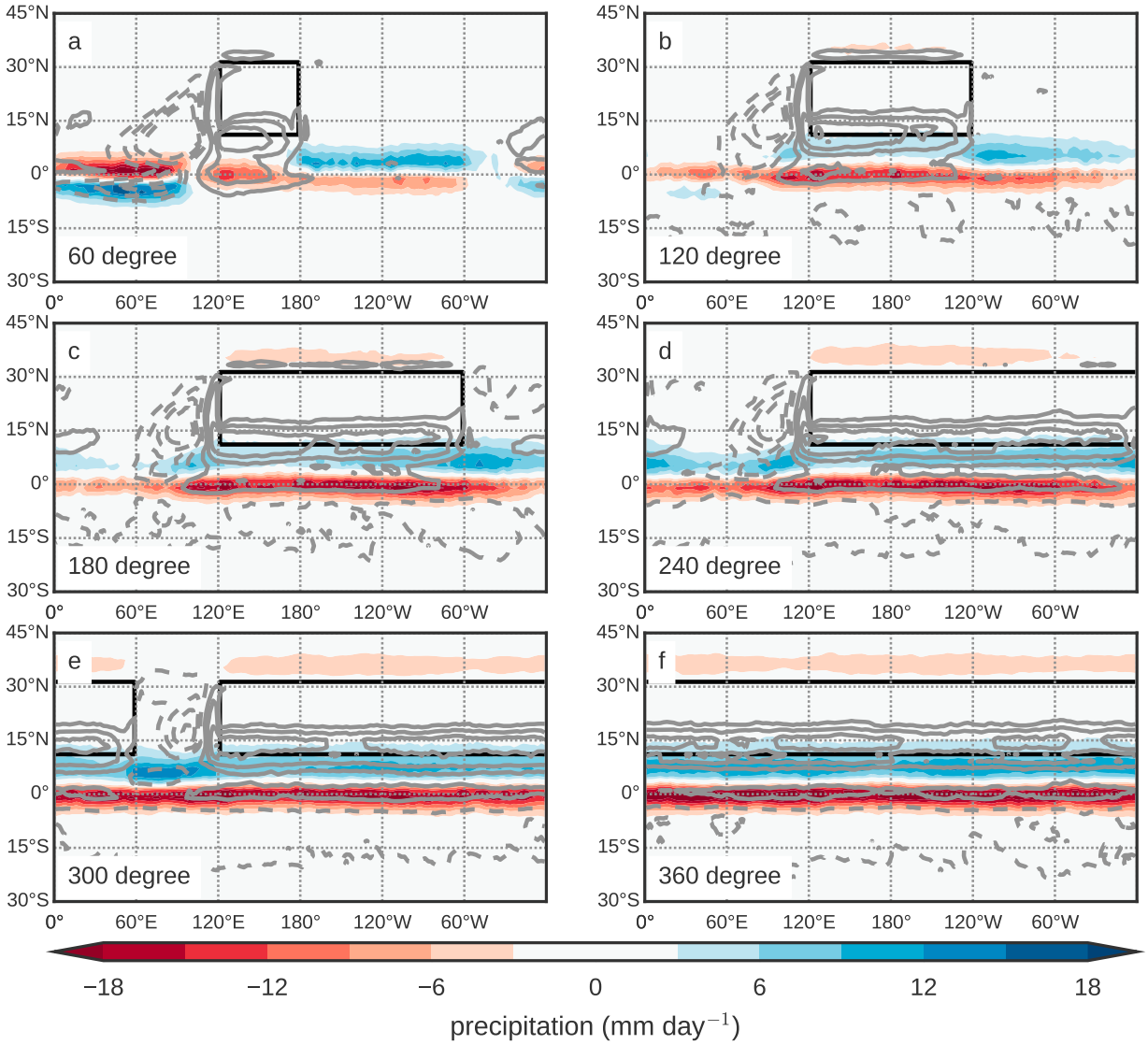

Figure 3. Changes relative to aquaplanet in precipitation (shading) and TOA net radiation (contours) for AM2.1 simulations with continents that span (a) 60°, (b) 120°, (c) 180°, (d) 240°, (e) 300°, and (f) 360° degrees of longitude. Net radiation is positive (solid) when it adds heat to the atmosphere and negative (dashed) when heat is lost. Contours are every 10 W m^{-2}.

As the continent's longitudinal extent increases, zonal-mean precipitation shifts farther into the NH (Figures 2c and 3). In the zonal mean, moisture convergence dominates the precipitation response; evaporation is smaller and of opposite sign (Figure 2a). Consistent with the zonal-mean energetic constraint, the change in atmospheric heat transport across the equator (AHT_{eq}) varies inversely with the zonal-mean NH-SH *P-E* change (Figure 2b). A deep anomalous Hadley circulation transports heat from NH to SH and moisture from SH to NH [e.g., *Kang et al.*, 2008], countering the decrease in evaporation (Figure 1f). Changes in AHT_{eq} accompany the changes in zonal-mean *P-E*, both of which increase with continental extent.

Although the zonal-mean shifts in *P-E* are consistent with the equatorial energy transport, the ITCZ does not shift uniformly and, in some simulation shifts, the regional precipitation shifts are in opposite directions. For example, the 60° continent simulation has almost no zonal-mean ITCZ shift and the greatest variability in the latitudinal ITCZ location at each longitude. To the west of the narrower continents, low stratus clouds form, which decreases SST and shifts precipitation southward there. Low stratus clouds are associated with subsidence and relatively low SST, which disfavors deep convection to the west of the continent. The SW cloud shading effect in this region decreases as the continent widens, and the SW cloud radiative effect (CRE) from these low clouds vanishes when the 360° continent covers the NH subtropical ocean (shading, Figure 4).

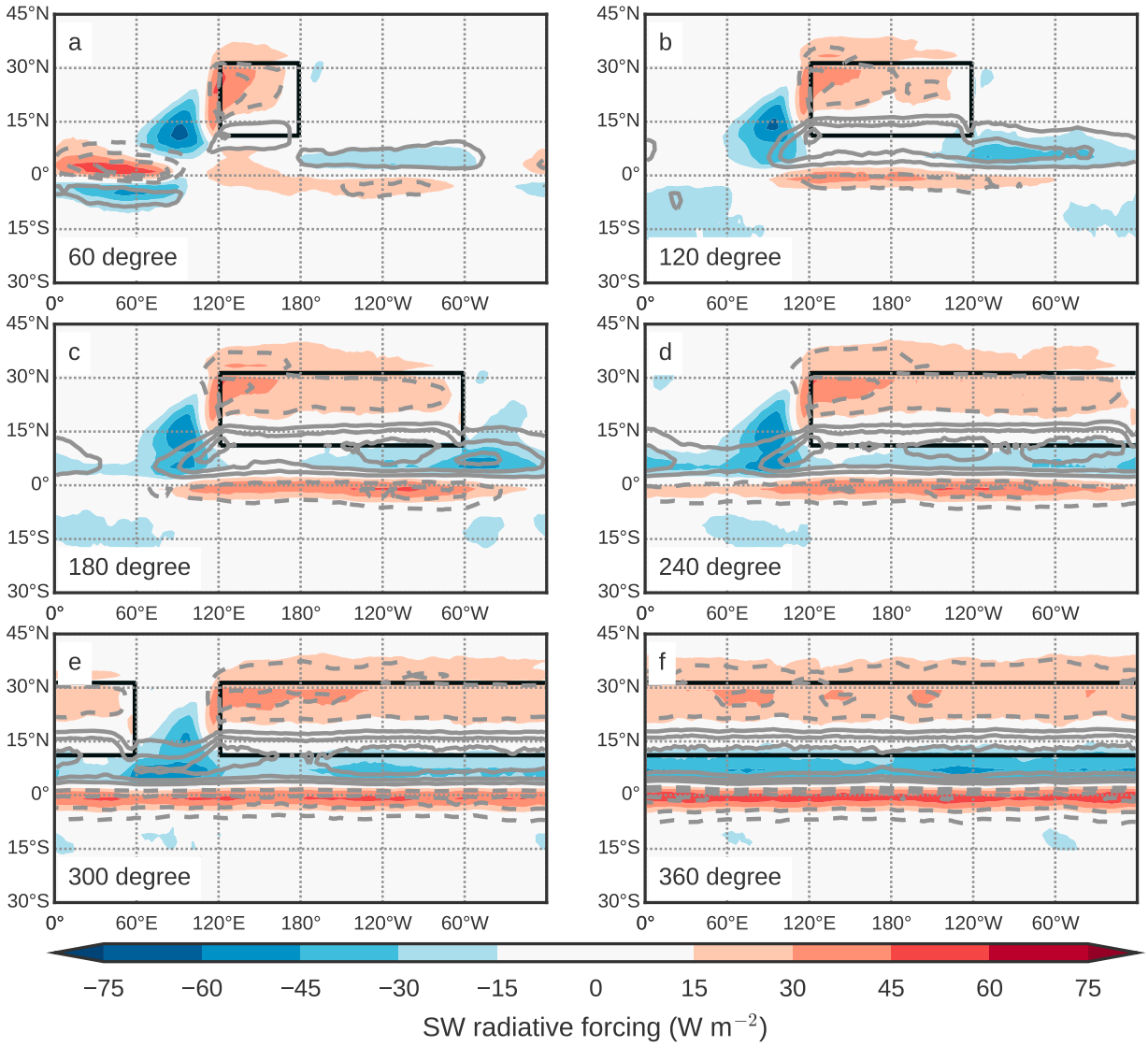

Figure 4. Changes in LW (contours) and SW (shading) for AM2.1 continent simulations. Changes are relative to the aquaplanet and for the same simulations in Figure 3. LW and SW radiations are positive where heat is added to the Earth. Contours and shading are every 15 W m^{-2}. Solid (dashed) contours are positive (negative).

The cross-equatorial SST gradient in this region decreases with continental extent due to decreasing deep tropical SH SST; as a result, the NH inhibition of precipitation is weakened.

In the continental region, precipitation shifts toward the hot land and decreases along the equator in association with anomalous ascent at the southern edge of the continent (Figures 1e and 1f). In the 60° simulation, precipitation decreases on the equator, but does not increase near the continent. As the continent widens, however, precipitation increases near the continent's southern edge and pushes west of the continent, decreasing the cloud-related southward shift there. This northward precipitation shift is almost proportional to the continent's longitudinal extent (Figures 2c, 3, and S5).

To the east of the continent, precipitation also shifts northward in all simulations, associated with anomalous southerlies along the equator (Figures 3 and S3). This wave-like response extends 120° east of the continent and, as a result, there is a nearly zonal northward ITCZ shift in simulations with a 240° or larger continent. For the narrower continent simulations, these anomalous southerlies are part of a stationary wave response, somewhat similar to the flow pattern from the off-equator line source heating in *Gill* [1980]. This similarity implies that the heating for the wave response could be due to the ITCZ shift itself. Although it is unclear what causes this ITCZ shift initially and why it is zonally limited, the fact that this wave response to the

continent's east does not occur in the GRaM simulations implies that radiative feedbacks are important for locally amplifying the ITCZ's equatorial asymmetry.

To quantify the zonal variability of the ITCZ location, we calculate the location of maximum precipitation at each longitude and then take the standard deviation of these locations (Figure 2e). The standard deviation of the ITCZ location for both the GRaM and AM2.1 simulations increases when the 60° continent is added and is smallest for the 360° continents where the shift toward the continent is zonal. The variability of the ITCZ location is related to the cloud-related southward precipitation shift to the west of the continent (Figures 2f, 3, and S4). As the continental extent is increased, the stratus clouds decrease and the SST in that region increases, and convection is not inhibited as strongly in the NH.

The circulation changes that affect moisture convergence and precipitation also affect the distribution of clouds and column water vapor, which alters the top-of-atmosphere (TOA) net radiation (Figure 3). Both the TOA longwave (LW) and shortwave (SW) radiations are impacted, and in many places, the pattern of their changes matches that of the precipitation anomalies (Figure 4). The pattern of anomalous LW and SW radiation tends to match that of the precipitation anomalies. However, because the combined LW CRE and clear-sky radiation (which increases column energy where precipitation increases) is larger than the shortwave (SW) CRE (which decreases column energy where precipitation increases), the pattern of anomalous TOA net radiation does not exactly match anomalous precipitation and is smaller in magnitude than either the LW or SW changes. TOA net downward radiation often increases where there is increased precipitation, following its zonal variations. Because the change in TOA net radiation from clouds and water vapor acts to increase the cross-equatorial energy transport, these radiative effects are a positive interhemispheric feedback that further increases the interhemispheric asymmetry of precipitation and the anomalous Hadley circulation [*Voigt et al.*, 2014]. Given the complexity of cloud parameterizations, other GCMs could have a different balance between TOA LW and SW.

The longitudinal extent of the continent has a nonlinear impact on the strength of the NH and SH Hadley circulations (Figure 2d). The addition of the 60° continent decreases the strength of both cells, as in the GRaM simulations. However, when the extent of the continent is 120°, the SH cell increases in strength, while the NH cell strength decreases. As the continent's extent increases further, the strength of the Hadley cells in both hemispheres increases and the strength of both cells in the 360° simulation is much stronger than that in the aquaplanet. In comparison to the GRaM simulations, the NH and SH overturning streamfunction vary more in the AM2.1 simulations.

4. Discussion

The response of tropical precipitation to an idealized continent can vary depending on the continent's geometry and the model's physical parameterizations. The change in the zonal-mean ITCZ location in GRaM simulations is mainly due to decreased evaporation over the new land surface. The development of a shallow land-driven circulation siphons moisture from the equatorial ITCZ toward the continent. The precipitation and circulation responses are confined to the NH in the band of longitudes where land is added and vary proportionally with the width of the continent. The circulation response is shallow and barely crosses the equator; the land-driven circulations in this simulation cannot be characterized as monsoonal [*Privé and Plumb*, 2007a]. In addition, the amount of SH precipitation is greater than the amount in the NH; the addition of a land surface in this model is not sufficient to develop a monsoon circulation, although testing with a seasonal cycle in this model is needed.

In contrast, the precipitation and circulation response in the AM2.1 simulations are not zonally confined to the continent and varies with continental extent. Where the continent is added, precipitation shifts northward toward the continent due to low-level convergence from an anomalous monsoon-like circulation. Precipitation also shifts northward to the east of the continent due to a stationary wave response. In the narrower continent simulations, precipitation shifts southward to the west of the continent due to increasing low clouds. These low clouds are associated with low SST and subsidence that disfavor precipitation. Although the surface heat flux forcing in the aquaplanet simulations of *Kang et al.* [2014] is of similar extent to our 60° continent, subtropical low clouds do not appear to form to the west of their forcing; the formation of these oceanic clouds requires dry air advected from over a land surface. As the continent widens in our simulations, the zone of precipitation that is drawn toward the continent also widens, and the southward shift to the west

of the continent weakens. When the continent is 240° or wider, precipitation shifts northward nearly zonally due to the wave response east of the continent (Figure 3). Figure S5 summarizes how much each regional precipitation shift contributes to the total zonal-mean shift in each AM2.1 simulation.

Changes in LW CRE, SW CRE, and clear-sky radiation accompany the precipitation shifts in all AM2.1 simulations. TOA LW outweighs the opposing SW CRE, and as a result, the column energy usually increases near locations where precipitation increases. In the zonal mean, energy is transported from the hemisphere with greater absorbed net radiation to the other hemisphere. Consequently, these changes in net radiation due to the cloud and clear-sky feedbacks amplify the northward shift of zonal-mean precipitation, a result confirmed in the cloud-locking simulations of *Voigt et al.* [2014]. Although this energetic constraint applies only in the zonal mean, the regionally opposing precipitation shifts in the narrower continent simulations are associated with a regional radiative balance that generally increases the net radiation near where precipitation increases. In simulations with narrower continents and an ITCZ location with large variability, the zonal-mean response can be understood as the sum of the regional responses.

Both the GRaM and AM2.1360° simulations feature a hot continent and anomalous ascent at the continent's southern edge, but the similarities end there. In the GRaM simulation, precipitation decreases near the continent due to evaporation, while in AM2.1, precipitation shifts toward the continent because of a larger and deeper overturning circulation response than that in the GRaM simulations. Anomalous cross-equatorial energy transport is northward in the GRaM simulation and southward in its AM2.1 counterpart. The difference in the sign of the cross-equatorial energy transport is likely due to the presence of cloud and water vapor feedbacks in AM2.1. When the continent heats up in either model, there is rising motion at the southern edge of the continent; in AM2.1 (but not in GRaM), deep clouds form in regions of ascent and high clouds extend away from the ITCZ, both of which increase the net column energy in the NH because the LW warming outweighs the SW cloud cooling. The additional net radiation from these radiative feedbacks warms the NH relative to the SH, which inverts the direction of the cross-equatorial energy transport from that in the GRaM simulation. This switch in the direction of cross-equatorial energy transport may not happen in a model with cloud parameterizations that have a different balance between SW and LW CRE [*Shaw et al.*, 2015].

For example, the model used in *Merlis et al.* [2013a, 2013b] is similar to AM2.1 but has a different representation of clouds. It includes the same 360° continent configuration, the same radiation scheme as AM2.1, and a bucket land model (simpler than LM2), but has prescribed liquid clouds. Our simulations do not have a seasonal cycle, which muddies the comparison of these two models, although *Maroon et al.* [2016] found that AM2.1 simulations with a seasonal cycle and a 60° continent had qualitatively similar results to simulations with annual-mean insolation. The annual-mean strength of the Hadley circulation increases in the 360° continent simulations with surface hydrology in *Merlis et al.* [2013b] as compared to the aquaplanet simulations in *Merlis et al.* [2013a], a result also found in our simulations. However, the 360° continent simulation in *Merlis et al.* [2013b] has a Hadley circulation with an annual-mean SH ascending branch, while our equivalent AM2.1 simulation has a NH ascending branch. Assuming changes in AHT_{eq} come from changes in Hadley circulation transport, then these two simulations also likely have oppositely-signed AHT_{eq}. These differing results could be related to the surface heat fluxes used in *Merlis et al.* [2013b] or to the different representations of clouds.

In these idealized simulations, precipitation shifts toward the continents that are 120° or wider, but for the 60° continent, only equatorial drying occurs; this result implies that the relatively smaller width of non-Asian continents (the Americas, Australia, and Africa) may be important for the weaker strength of their monsoons relative to the Asian monsoon. The relatively simple configuration used in this study is limited if trying to understand the full complexity of the observed tropical overturning circulation [*Karnauskas and Ummenhofer*, 2014]. However, the surprisingly complex climate response in these configurations is proof that more study is needed with continent geometries that gradually approach a realistic configuration.

Acknowledgments

E.A.M. was supported by an NDSEG fellowship and IGERT Program on Ocean Change traineeship. D.M.W.F was supported by NSF grants AGS-1359464 and PLR-1341497, and a UW Royalty Research Fund grant. We thank two anonymous reviewers for constructive feedback, Jacob Scheff for assistance with the AM2.1 model setup, and Sarah Kang, Cecilia Bitz, and Ángel Adames-Corraliza for helpful discussions. Model output from this study is available at http://atmos.washington.edu/emaroon/continentwideningoutput.

References

Back, L. E., and C. S. Bretherton (2006), Geographic variability in the export of moist static energy and vertical motion profiles in the tropical Pacific, *Geophys. Res. Lett.*, *33*, L17810, doi:10.1029/2006GL026672.

Boos, W. R., and Z. Kuang (2010), Dominant control of the South Asian monsoon by orographic insulation versus plateau heating, *Nature*, *463*, 218–222.

Bordoni, S., and T. Schneider (2008), Monsoons as eddy-mediated regime transitions of the tropical overturning circulation, *Nature Geosci.*, *1*, 515–519.

Broccoli, A. J., K. A. Dahl, and R. J. Stouffer (2006), Response of the ITCZ to Northern Hemisphere cooling, *Geophys. Res. Lett.*, *33*, L01702, doi:10.1029/2005GL024546.

Chao, W. C., and B. Chen (2001), The origin of monsoons, *J. Atmos. Sci.*, *58*(22), 3497–3507.
Chiang, J. C. H., and C. M. Bitz (2005), Influence of high latitude ice cover on the marine Intertropical Convergence Zone, *Clim. Dyn.*, *25*, 477–496.
Dima, I. M., and J. M. Wallace (2003), On the seasonality of the Hadley Cell, *J. Atmos. Sci.*, *60*, 1522–1527.
Donohoe, A., J. Marshall, D. Ferreira, and D. McGee (2013), The relationship between ITCZ location and cross-equatorial atmospheric heat transport: From the seasonal cycle to the Last Glacial Maximum, *J. Clim.*, *26*, 3597–3618.
Frierson, D. M. W., I. M. Held, and P. Zurita-Gotor (2006), A gray radiation aquaplanet moist GCM. Part I: Static stability and eddy scale, *J. Atmos. Sci*, *63*, 2548–2566.
Frierson, D. M. W., and Y.-T. Hwang (2012), Extratropical influence on ITCZ shifts in slab ocean simulations of global warming, *J. Clim.*, *25*, 720–733.
Frierson, D. M. W., Y.-T. Hwang, N. S. Fučkar, R. Seager, S. M. Kang, A. Donohoe, E. A. Maroon, X. Liu, and D. S. Battisti (2013), Contribution of ocean overturning circulation to tropical rainfall peak in the Northern Hemisphere, *Nature Geosci.*, *49*(14), 1233–1241.
Gadgil, S. (2003), The Indian monsoon and its variability, *Annu. Rev. Earth Planet. Sci.*, *31*, 429–467.
Geophysical Fluid Dynamics Laboratory Global Atmospheric Model Development Team (2004), The new GFDL global atmosphere and land model AM2 LM2: Evaluation with prescribed SST simulations, *J. Clim.*, *17*, 4641–4673.
Gill, A. E. (1980), Some simple solutions for heat-induced tropical circulation, *Q. J. R. Meteorol. Soc.*, *106*, 447–462.
Hahn, D. G., and S. Manabe (1975), The role of mountains in the South Asian monsoon circulation, *J. Atmos. Sci.*, *32*, 1515–1541.
Held, I. M., and A. Y. Hou (1980), Nonlinear axially symmetric circulations in a nearly inviscid atmosphere, *J. Atmos. Sci.*, *37*(3), 515–533.
Hwang, Y.-T., D. M. W. Frierson, and S. M. Kang (2013), Anthropogenic sulfate aerosol and the southward shift of tropical precipitation in the late 20th century, *Geophys. Res. Lett*, *40*, 2845–2850, doi:10.1002/grl.50502.
Joshi, M. M., J. M. Gregory, M. J. Webb, D. M. H. Sexton, and T. C. Johns (2008), Mechanisms for the land/sea warming contrast exhibited by simulations of climate change, *Clim. Dyn.*, *30*, 455–465.
Kang, S. M., I. M. Held, D. M. W. Frierson, and M. Zhao (2008), The response of the ITCZ to extratropical thermal forcing: Idealized slab-ocean experiments with a GCM, *J. Clim.*, *21*(14), 3521–3532.
Kang, S. M., D. M. W. Frierson, and I. M. Held (2009), The tropical response to extratropical thermal forcing in an idealized GCM: The importance of radiative feedbacks and convective parameterization, *J. Atmos. Sci.*, *66*(9), 2812–2827.
Kang, S. M., I. M. Held, and S.-P. Xie (2014), Contrasting the tropical responses to zonally asymmetric extratropical and tropical thermal forcing, *Clim. Dyn.*, *42*, 2033–2043.
Karnauskas, K. B., and C. C. Ummenhofer (2014), On the dynamics of the Hadley circulation and subtropical drying, *Clim. Dyn.*, *42*, 2259–2269.
Lindzen, R. S., and A. Y. Hou (1988), Hadley circulations for zonally averaged heating centered off the equator, *J. Atmos. Sci.*, *45*, 2416–2427.
Manabe, S. (1969), Climate and the ocean circulation. 1. The atmospheric circulation and the hydrology of the Earth's surface, *Mon. Weather Rev.*, *97*, 739–774.
Maroon, E. A., D. M. W. Frierson, S. M. Kang, and J. Scheff (2016), The precipitation response to an idealized subtropical continent, *J. Clim.*, *29*, 4543–4564.
Merlis, T. M., T. Schneider, S. Bordoni, and I. Eisenman (2013a), Hadley circulation response to orbital precession. Part I: Aquaplanets, *J. Clim.*, *26*, 740–753.
Merlis, T. M., T. Schneider, S. Bordoni, and I. Eisenman (2013b), Hadley circulation response to orbital precession. Part II: Subtropical continent, *J. Clim.*, *26*, 754–771.
Milly, P. C. D., and A. B. Shmakin (2002), Global modeling of land water and energy balances. Part I: The Land Dynamics (LaD) model, *J. Hydrometeorol.*, *3*, 283–299.
Plumb, R. A., and A. Y. Hou (1992), The response of a zonally symmetric atmosphere to subtropical thermal forcing: Threshold behavior, *J. Atmos. Sci.*, *49*, 1790–1799.
Privé, N. C., and R. A. Plumb (2007a), Monsoon dynamics with interactive forcing. Part I: Axisymmetric studies, *J. Atmos. Sci.*, *64*, 915–934.
Privé, N. C., and R. A. Plumb (2007b), Monsoon dynamics with interactive forcing. Part II: Impact of eddies and asymmetric geometries, *J. Atmos. Sci.*, *64*, 1431–1442.
Scheff, J. (2014), Understanding the responses of precipitation, evaporative demand, and terrestrial water availability to planetary temperature in climate models, PhD dissertation, 199 pp., Department of Atmospheric Sciences, Univ. of Washington, Seattle. [Available at: http://www.ldeo.columbia.edu/jscheff/JacobScheffUWDissertation.pdf.]
Schneider, T., T. Bischoff, and G. H. Haug (2014), Migrations and dynamics of the intertropical convergence zone, *Nature*, *513*, 45–53.
Shaw, T. A., A. Voigt, S. M. Kang, and J. Seo (2015), Response of the Intertropical Convergence Zone to zonally-asymmetric subtropical surface forcings, *Geophys. Res. Lett.*, *42*, 9961–9969, doi:10.1002/2015GL066027.
Shi, X., and D. R. Durran (1992), The response of orographic precipitation over idealized mid-latitude mountains due to global increases in CO_2, *J. Clim.*, *27*, 3938–3956.
Sobel, A. H., J. Nilsson, and L. M. Polvani (2001), The weak temperature gradient approximation and balanced tropical moisture waves, *J. Atmos. Sci.*, *58*, 3650–3665.
Voigt, A., S. Bony, J.-L. Dufresne, and B. Stevens (2014), The radiative impact of clouds on the shift of the Intertropical Convergence Zone, *Geophys. Res Lett.*, *41*, 4308–4315, doi:10.1002/2014GL060354.